Research Square

Preprints are preliminary reports that have not undergone peer review.
They should not be considered conclusive, used to inform clinical practice,
or referenced by the media as validated information.

Intrinsic transverse magnetic nonreciprocal response in a noncollinear antiferromagnet

Lin Jiao

lin.jiao@zju.edu.cn

Zhejiang University https://orcid.org/0000-0002-8343-0190

Hengrui Gui

Zhejiang University

Ziming Wang

Chongqing University

Zekai Shi

Zhejiang University

Jiawen Zhang

Zhejiang University

Yongjian Li

Zhejiang University

Ke Xia

Southeast University https://orcid.org/0000-0002-0246-3944

Yu Liu

Zhejiang University

Jinglei Zhang

Anhui Key Laboratory of Condensed Matter Physics at Extreme Conditions, High Magnetic Field Laboratory, HFIPS, Chinese Academy of Sciences, Hefei 230031, China

Taishi Chen

Southeast University https://orcid.org/0000-0003-1827-6614

Huiqiu Yuan

Zhejiang University https://orcid.org/0000-0002-9787-4884

Lun-Hui Hu

Zhejiang University https://orcid.org/0000-0002-0376-3367

Article

Keywords:

Posted Date: July 1st, 2026

DOI: https://doi.org/10.21203/rs.3.rs-10128837/v1

License: This work is licensed under a Creative Commons Attribution 4.0 International License.
Read Full License

Additional Declarations: There is **NO** Competing Interest.

Intrinsic transverse magnetic nonreciprocal response in a noncollinear antiferromagnet

Hengrui Gui[1†], Zi-Ming Wang[1,2†], Zekai Shi[1], Jiawen Zhang[1], Yongjian Li[1], Ke Xia[3], Yu Liu[1], Jinglei Zhang[4], Taishi Chen[3*], Huiqiu Yuan[1,5,6*], Lun-Hui Hu[1*], Lin Jiao[1*],

[1]New Cornerstone Science Laboratory, Center for Correlated Matter and School of Physics, Zhejiang University, Hangzhou 310058, China.

[2]Department of Physics and Chongqing Key Laboratory for Strongly Coupled Physics, Chongqing University, Chongqing 400044, China.

[3]Key Laboratory of Quantum Materials and Devices of Ministry of Education, School of Physics, Southeast University, Nanjing 211189, China

[4]Anhui Province Key Laboratory of Condensed Matter Physics at Extreme Conditions, High Magnetic Field Laboratory of the Chinese Academy of Sciences, Hefei 230031, Anhui, China

[5]Institute of Fundamental and Transdisciplinary Research, Zhejiang University, Hangzhou 310058, China.

[6]State Key Laboratory of Silicon and Advanced Semiconductor Materials, Zhejiang University, Hangzhou 310058, China.

[*]Corresponding author. Email: chentaishi@seu.edu.cn; hqyuan@zju.edu.cn; lunhui@zju.edu.cn; lin.jiao@zju.edu.cn

[†]These authors contributed equally to this work.

Nonreciprocal responses transform broken symmetries into direction-dependent functionality, while a nonreciprocal response encoded directly in static magnetic response of an ordered magnet has not been realized. Here we reveal an intrinsic transverse magnetic nonreciprocity in the noncollinear antiferromagnet Mn_3Ge. Using torque magnetometry, we observe a pronounced transverse torque that is odd under magnetic-field reversal, in sharp contrast to the reciprocal response of conventional magnets. A concomitant even-in-field planar Hall response emerges at the same low temperature around 210 K, well below the Néel temperature. Together, these measurements reveal a field-reversal-even transverse magnetic response in which opposite fields select symmetry-related, rather than time-reversed, noncollinear antiferromagnetic states. We attribute this behavior to spin-orbit-coupling-induced breaking of spin space group symmetry, which locks the noncollinear spin texture and its net magnetization to the lattice. These results establish a nonreciprocal magnetic response as a distinct collective response of chiral antiferromagnets, extending nonreciprocal phenomena beyond charge-current-based transport.

Nonreciprocity is a general manifestation of broken symmetry, in which a system responds differently to opposite directions of motion, propagation, or driving. It underlies rectification in semiconductor junctions and has recently expanded into quantum materials through electrical magnetochiral anisotropy, nonlinear optical responses, superconducting diode effects, and nonreciprocal collective excitations (*1–3*). However, these known examples largely involve transport or propagation properties of carriers (*1–9*). By contrast, the static transverse/longitudinal magnetic response of a material to external magnetic field has conventionally been assumed reciprocal: reversing the field direction simply reverses the magnetization, leaving the magnitude of the resulting magnetization unchanged without directional asymmetry. Whether nonreciprocity can be encoded in the magnetic response of materials under field reversal remains an open question.

Unconventional antiferromagnets, with their rich broken symmetries (*10–13*), may provide a natural setting to search for exotic response. In noncollinear chiral antiferromagnets, for example, the handedness of a noncollinear spin texture becomes a symmetry-relevant degree of freedom, breaking time-reversal symmetry without producing a large net magnetization. This enables anoma-

lous transverse responses and ferroic multipolar order that are controlled by magnetic symmetry rather than conventional ferromagnetism (*14–18*). In the limit of negligible spin-orbit coupling (SOC), spin-space-group symmetries enforce compensated spin magnetization even in a time-reversal broken noncollinear state. SOC reduces this symmetry by locking spin space to the lattice, simultaneously enabling anomalous Hall responses and net magnetization (*19–23*). This symmetry hierarchy suggests that SOC may affect not only Hall-type transport, but also the field-reversal symmetry of the magnetic response (*24*).

A paradigmatic family of noncollinear chiral antiferromagnets is Mn_3X (X = Sn, Ge, Ga), where Mn moments form a 120° spin texture on kagome layers (see Figs. 1A and B) (*25–29*). Among this family, Mn_3Sn has become a model system after the discovery of a large room-temperature anomalous Hall effect in a nearly compensated antiferromagnet (*30*). This discovery has stimulated extensive studies of magnetic Weyl fermions, ferroic octupole domains, spin-orbit-torque switching, coherent electrical driving, and field-free switching of chiral antiferromagnetic order (*31–41*). By comparison, Mn_3Ge and Mn_3Ga, although known to host sizable anomalous Hall responses, have been less explored as platforms for symmetry-controlled antiferromagnetic functionality beyond Hall-type transport (*42–44*). Mn_3Ge is particularly relevant in this context because theory predicts that SOC generates a sizable net magnetization (*19, 22*), yet the intrinsic nature of its magnetic response (e.g., torque) remains unsettled.

This raises a fundamental question: akin to the well-established SOC-driven magnetochiral anisotropy in nonmagnetic materials (*3*), can SOC-induced net magnetization in unconventional magnetic materials generate new type of nonreciprocal behavior in magnetic/torque response? Here, we address this question by showing an intrinsic transverse magnetic nonreciprocal response in Mn_3Ge. By employing in-plane torque magnetometry and planar Hall measurements, we find a concomitant even-in-field transverse magnetization component that emerges well inside the chiral antiferromagnetic phase. Together with symmetry analysis, these results point to a pinned transverse magnetization within the kagome plane, generated by SOC-induced breaking of spin-space-group symmetry. Mn_3Ge therefore establishes chiral antiferromagnets as a platform for nonreciprocal magnetic functionality, extending nonreciprocal phenomena from transport and wave propagation to the collective magnetic response of an ordered quantum material.

Observation of a nonreciprocal transverse torque

Torque magnetometry is particularly sensitive to the magnetization component transverse to the applied field (*45–49*). For a fixed in-plane field direction, the measured torque can be written as $\boldsymbol{\tau} \propto \mathbf{M} \times \mathbf{H}$. For a hysteretic magnetic response, the magnetic state can depend on the field-sweep protocol. We denote the field-increasing and field-decreasing branches as forward (f) and backward (b), respectively. In the low-field regime, the branch-resolved magnetization may be expanded as $\mathbf{M}_{f,b}(\mathbf{H}) = \mathbf{M}^0_{f,b} + \chi_{f,b} \cdot \mathbf{H}$, where $\mathbf{M}^0_{f,b}$ are the spontaneous components and $\chi_{f,b}$ are the corresponding susceptibility tensors (*50*). This two-branch description reflects the history dependence of a magnetically ordered state, where different magnetic configurations can be selected along opposite field-sweep directions. The field-reversal symmetry of the magnetization can be classified by the branch-exchanged even and odd components: $\mathbf{M}_{\text{even}}(\mathbf{H}) = [\mathbf{M}_f(\mathbf{H}) + \mathbf{M}_b(-\mathbf{H})]/2$, and $\mathbf{M}_{\text{odd}}(\mathbf{H}) = [\mathbf{M}_f(\mathbf{H}) - \mathbf{M}_b(-\mathbf{H})]/2$. In conventional reciprocal hysteresis, as in ferromagnets, the spontaneous magnetization selected by opposite sweep histories reverses under field reversal, $\mathbf{M}^0_f \simeq -\mathbf{M}^0_b$, so that the field-reversed branches satisfy $\mathbf{M}_f(\mathbf{H}) \simeq -\mathbf{M}_b(-\mathbf{H})$ for the parallel component (i.e. $\mathbf{M}_{\text{even}}(\mathbf{H}) \simeq 0$), or equivalently $\boldsymbol{\tau}_f(\mathbf{H}) \simeq \boldsymbol{\tau}_b(-\mathbf{H})$ for the transverse torque response. By contrast, an unconventional response can arise if a transverse spontaneous component remains pinned to the lattice and does not reverse with the applied field.

To make this connection explicit, we focus on the magnetization component perpendicular to the applied field. For a fixed field direction, the transverse components on the two sweep branches give the scalar torque:

$$\tau_{f,b}(H) \simeq H\left(M^{0,\perp}_{f,b} + \chi^{\perp}_{f,b} H\right). \tag{1}$$

If the transverse component is pinned by the lattice and remains non-reversed under field reversal, i.e., $M^{0,\perp}_f \simeq M^{0,\perp}_b$, the linear term $HM^{0,\perp}$ produces an odd-in-field torque. In this case, $\tau_f(H) \neq \tau_b(-H)$, which defines the general magnetic nonreciprocal response. Remarkably, at low fields, one expects $\tau_f(H) \simeq -\tau_b(-H)$.

Our measurement configuration is shown in Fig. 1C. The sample was mounted on a piezoresistive cantilever, and the magnetic field was applied within the kagome plane. The resulting torque is therefore along the sample c-axis, making the measurement sensitive to the in-plane transverse magnetization component. Small mounting-induced misalignment is estimated to be

less than 5° and does not affect the field-reversal symmetry analysis discussed in the following. Figure 1D compares representative torque responses of conventional hysteretic magnets with that of Mn_3Ge. The ferromagnet Fe_3GeTe_2 and the noncollinear antiferromagnet Mn_3Ga both show conventional butterfly-shaped hysteresis loops, for which the two branches approximately satisfy $\tau_f(H) \simeq \tau_b(-H)$ (*44, 50–52*). Previous torque measurements on Mn_3Sn also reported a conventional behavior (*47*). These examples also demonstrate that magnetic hysteresis alone does not imply magnetic nonreciprocity.

In sharp contrast, Mn_3Ge exhibits a qualitatively different torque response at low temperature. At $T = 10$ K and with the field applied within the kagome plane, the low-field torque loop is dominated by an odd-symmetric component under field reversal: the forward branch at positive field is not reproduced by the backward branch at negative field; instead, one clearly finds $\tau_f(H) \simeq -\tau_b(-H)$ at low H. According to Eq. (1), this behavior implies an even-in-field transverse magnetization component, consistent with a transverse moment that remains pinned rather than reversing with the applied field. At sufficiently large fields, the anomalous low-field hysteresis is suppressed and the branches merge into a more conventional field-polarized response, indicating that the nonreciprocal signal is associated with a low-field magnetic configuration rather than with a simple background torque. We next examine its angular and temperature dependence to establish its intrinsic origin.

Field-direction control of the nonreciprocal torque

Having established a nonreciprocal transverse torque for an in-plane magnetic field, we next examine how this response depends on field orientation within the kagome plane. For a spontaneous in-plane moment $\mathbf{M}^0$ locked to the lattice, the nonreciprocal torque is expected to scale as $\tau_{\mathrm{NR}}(\theta, H) \propto H|\mathbf{M}^0| \sin(\theta - \theta_M)$, where θ is the field angle within the kagome plane and θ_M denotes the direction of $\mathbf{M}^0$. Thus the nonreciprocal torque should change sign upon rotating the field and should vanish when the applied field is nearly parallel to the pinned moment.

Figure 2A shows representative torque hysteresis loops measured at 10 K with the field applied along four principal directions, $+y$, $+x$, $-y$, and $-x$. In all cases, the low-field torque response violates the reciprocal relation with both the magnitude and polarity of this violation depending on field orientation. The torque loops for $\mathbf{H} \parallel +y$ and $-x$ are nearly identical, whereas those for

$\mathbf{H} \parallel -y$ and $+x$ form the opposite pair. This sign pattern indicates that the response is not a scalar hysteretic background, but instead reflects the projection of a vector-like transverse magnetization onto the direction perpendicular to the applied field.

To resolve the angular evolution more continuously, we measured $\tau(H, \theta)$ with finer angular steps, as shown in Fig. 2B. When the field is rotated from $\theta = 30^\circ$ to 60°, the low-field torque evolves from a nearly reciprocal butterfly-shaped loop into a clearly nonreciprocal loop. The nearly reciprocal response near $\theta = 30^\circ$ should not be interpreted as the disappearance of the underlying nonreciprocal magnetic state. Rather, it corresponds to an angular node of the torque signal, where the applied field is nearly parallel to the pinned transverse moment and the cross product $\mathbf{M}^0 \times \mathbf{H}$ is strongly suppressed. This also explains why previous torque measurements performed along limited field directions only observe predominantly conventional responses (*49*).

We further quantify the transverse moment by fitting the low-field scalar torque at each angle to Eq. (1), which derives the transverse moment $M^{0,\perp}_{f,b}(\theta)$. As summarized in Fig. 2C, $M^{0,\perp}_{f}$ and $M^{0,\perp}_{b}$ retain the same sign in the nonreciprocal angular sectors, demonstrating that the transverse component does not reverse with field reversal. By contrast, near the angular node where the measured torque becomes nearly reciprocal, $M^{0,\perp}$ become small or branch-opposite, as expected when the conventional susceptibility contribution dominates. Phenomenologically, this nonreciprocal torque response in Mn_3Ge belongs to the same class as electrical magnetochiral anisotropy, where the nonreciprocal resistance depends on the dot product between current and magnetic field: $R(\mathbf{I}, \mathbf{H}) = R_0 + \gamma(\mathbf{I} \cdot \mathbf{H}) + \beta(H)^2$ (*6, 8*). In that case, γ arises from SOC (*3*). When $\mathbf{H}$ is rotated perpendicular to $\mathbf{I}$, the reciprocal resistance dominates. As discussed later, SOC is a key driving force for the intrinsic nonreciprocal torque response reported here. Our finding suggests that analogous nonreciprocal magnetic responses may arise more broadly in unconventional antiferromagnetic systems.

Finally, we extracted the low-field torque amplitudes at $H^0 = 0.5$ T to characterize the full angular dependence. The forward-branch signal $\tau_f(+H^0, \theta)$ and the field-reversed backward-branch signal $\tau_b(-H^0, \theta)$ follow nearly sinusoidal angular dependences with opposite signs, consistent with the cross-product form of a pinned in-plane moment (Fig. 2D). The angular node occurs near $\theta \simeq 30^\circ$, again, indicating that the spontaneous transverse moment is oriented approximately 30° away from the $+y$ axis within the kagome plane. The emergence of a well-defined node, sign

reversal, and sinusoidal angular dependence provides strong evidence that the nonreciprocal torque originates from an intrinsic pinned transverse magnetization rather than from sample misalignment or a conventional hysteretic background.

Low-temperature onset of the nonreciprocal torque

Having established the vector nature of the nonreciprocal torque, we next examine its temperature evolution. We focus on two in-plane field directions, $\mathbf{H} \parallel -x$ and $\mathbf{H} \parallel +y$, see Figs. 3A and B. At high temperatures but below T_N, the torque response is even symmetric without hysteresis under field reversal. Upon cooling, however, an antisymmetric low-field torque loop gradually develops. The deviation from the reciprocal relation becomes clearly visible below approximately 210 K for both field directions. To quantify this onset, we define the low-field nonreciprocal torque amplitude as

$$\Delta\tau_{\mathrm{NR}}(T) = \frac{1}{2}\left|\tau_f^{\mathrm{peak}}(T) - \tau_b^{\mathrm{dip}}(T)\right|, \tag{2}$$

where τ_f^{peak} and τ_b^{dip} are the characteristic peak and dip values of the forward and field-reversed backward branches in the low-field regime. This quantity estimates the magnitude of the field-reversal-odd torque component introduced above. As summarized in Fig. 3C, $\Delta\tau_{\mathrm{NR}}$ shows a signature temperature around 210 K.

Notably, this characteristic temperature lies far below the T_N of Mn_3Ge and is not accompanied by anomalies in conventional magnetization, electrical or thermal transport measurements in previous reports (*29,42,43,53*). A natural interpretation is that thermal fluctuations and thermally assisted domain reconfiguration suppress the coherent pinned transverse response at elevated temperatures. In this regime, different low-field magnetic configurations can be sampled during field sweeping, and their transverse torque contributions are averaged out macroscopically. Upon cooling, such fluctuations are progressively frozen, allowing a homogeneous pinned transverse component to dominate the low-field response. This scenario is consistent with the sharp growth of $\Delta\tau_{\mathrm{NR}}$ below $\sim$ 210 K and with the absence of a corresponding signature of structural transition [see Fig. S2]. This is very different from the chiral domain wall effects observed in Mn_3Sn and Mn_3Ge, which are closely associated with the noncollinear antiferromagnetic order and its domain-wall dynamics, and their onset is therefore at T_N (*54, 55*). Consequently, we argue that the robust nonreciprocal

response reveals an intrinsic magnetic response of the homogeneous state once thermally induced domain fluctuations are fully quenched. This argument is further supported by the fact that our new generation Mn_3Ge sample is very clean (*56*).

Planar Hall signature of nonreciprocal magnetic response

To further probe the bulk nature of the transverse nonreciprocal magnetization, we measured the Hall response (ρ^{xz}) of Mn_3Ge with magnetic field rotating from y to x-axis and current flow along z-axis. In this configuration, $\mathbf{H} \parallel y$ is primarily sensitive to the AHE contribution to ρ^{xz}, whereas $\mathbf{H} \parallel x$ suppresses the conventional Hall geometry and makes the measurement sensitive to a PHE-like transverse response. Figures 4A and 4B compare the angular evolution of $\rho^{xz}(H)$ at 300 K and 10 K, respectively. At high temperatures, only AHE (odd component of $\rho^{xz}(H)$) is observed, which was well characterized in previous studies and was understood in terms of weak ferromagnetism along y-axis (*29, 42, 43*). The residual AHE at 90° may be due to a small angle misalignment or domain nucleation (*55*). By contrast, at 10 K an additional field-reversal-even transverse response appears as the field approaches $\mathbf{H} \parallel x$. This low-temperature even-in-field signal is the transport counterpart of the nonreciprocal torque response.

To separate the two contributions quantitatively, we decompose the measured transverse resistivity into field-reversal-odd and field-reversal-even components using the same branch-exchange operation introduced for the torque: $\rho_{\mathrm{odd}}(H) = [\rho_f^{xz}(H) - \rho_b^{xz}(-H)]/2$ and $\rho_{\mathrm{even}}(H) = [\rho_f^{xz}(H) + \rho_b^{xz}(-H)]/2$. In the present measurement geometry, ρ_{odd} mainly tracks the AHE-like response, whereas ρ_{even} captures the PHE-like transverse response associated with the field-reversal-even magnetic component. Figure 4C shows the temperature evolution of $\rho^{xz}(H)$ for $\mathbf{H} \parallel x$, where the PHE-like contribution is most clearly resolved. The corresponding ρ_{odd} and ρ_{even} components are plotted in Figs. 4D and 4E. The odd component remains visible over a broad temperature range, consistent with the persistence of the chiral antiferromagnetic order. In contrast, the even component is negligible at high temperature and emerges only below approximately 210 K. To quantify this evolution, we define the ratio $R_{\mathrm{even}} = S_{\mathrm{even}}/S_{\mathrm{odd}}$, where S_{even} and S_{odd} denote the hysteretic loop areas of ρ_{even} and ρ_{odd}, respectively. As shown in Fig. 4F, R_{even} increases rapidly below ~210 K, matching the onset temperature of the nonreciprocal torque amplitude $\Delta\tau_{\mathrm{NR}}$ in Fig. 3. This

agreement demonstrates that the torque and PHE measurements detect the same low-temperature transverse magnetic-response regime.

Therefore, the PHE provides a complementary transport signature of the same underlying symmetry breaking magnetic phase. Again, the temperature dependence of the PHE observed here contrasts sharply with previously reported domain-wall-induced PHE (*54, 55*). As the domain wall induced PHE is closely related to the noncollinear AFM order, its onset temperature coincides with the Néel temperature. Meanwhile the domain wall induced PHE should, and indeed, show pronounced memory effect which is absent in our case (see Exclude domain wall effect in Supplementary Text). We believe that the vanished PHE above ~210 K evidences an intrinsic nonreciprocal magnetic response of the ultra-clean bulk crystal.

SOC-induced spin-space group symmetry breaking

We next provide a possible theoretical understanding and find that the underlying mechanism originates from SOC-induced spin-space group symmetry breaking that generates a spontaneous transverse magnetization $\mathbf{M}^0$ within the kagome plane (*57*). As illustrated in Fig. 5A, the system adopts distinct magnetic configurations under positive and negative fields that are related by a $\pi/3$ global rotation of the AFM configuration—evidenced by the global angle evolving from $\theta_g = -\pi/6$ to $\pi/6$ as the field reverses. In Supplementary Text, the free energy calculations as a function of θ_g confirm that the $+\mathbf{H}$ and $-\mathbf{H}$ states correspond to distinct local minima separated by a spin-flop-like transition of $\pi/3$, consistent with SOC-induced magnetic anisotropy (*22*). The corresponding magnetization (orange arrows) is constrained by a two-fold rotation symmetry axis to remain parallel to a fixed crystallographic direction regardless of field polarity. This symmetry pinning prevents the calculated $\mathbf{M}^0$ from reversing with the field, yielding the even-in-field magnetization (Fig. 5B) and the corresponding odd-in-field torque responses (Fig. 5C), in good agreement with our experiments. We emphasize that the total magnetization comprises both spin and orbital contributions (*19*); by symmetry, SOC couples these components such that they align collinearly along the two-fold rotation axis, effectively reinforcing the nonreciprocal response rather than canceling it.

In the context of chiral noncollinear antiferromagnets, Mn_3Ge distinguishes itself from its isostructural counterpart Mn_3Sn through the magnitude of SOC-induced spontaneous magnetiza-

tion. Mn_3Ge stabilizes a robust spontaneous transverse magnetization that remains pinned during field reversal, whereas Mn_3Sn exhibits conventional reciprocal behavior—a difference that may be due to the negligible magnetization of Mn_3Sn (*19*). This material-specific difference suggests that the emergence of magnetic nonreciprocity depends sensitively on the interplay among spin-orbit coupling, magnetic anisotropy, and the field-dependent energy landscape of the noncollinear spin texture.

More broadly, nonreciprocity represents a functional property that enables directional device operation, with manifestations spanning from pure electrical rectification in semiconductor p-n junctions, to magnetochiral anisotropy requiring the cooperation of both electric and magnetic fields (*3*), and finally to the phenomena we establish here: a purely magnetic-field-induced nonreciprocal response. Therefore, Mn_3Ge realizes a new form of nonreciprocity, where directional hysteresis can emerge solely from the interplay between chiral spin order and SOC, without requiring charge currents—offering compelling opportunities for antiferromagnetic spintronics. Furthermore, the angular dependence of the nonreciprocal response (Fig. 2) implies that the system can function as a directional magnetic sensor, sensitive not merely to field magnitude but to the history and orientation of field application.

In summary, we have identified an intrinsic nonreciprocal transverse magnetization in the kagome antiferromagnet Mn_3Ge. Torque magnetometry reveals odd-symmetric hysteresis loops that deviate fundamentally from reciprocal magnetic responses. The transverse magnetization is spontaneous, retains its sign under field reversal, and orients approximately 30° away from the crystallographic y-axis. The nonreciprocal response emerges only below ~210 K, indicating an additional low-temperature magnetic-response regime within the chiral antiferromagnetic phase, distinct from the Néel transition iteself. Theoretical analysis attributes this behavior to spin-orbit-induced spin-space group symmetry breaking, which enables a chirality-locked coherent rotation of the noncollinear spin texture. Upon field reversal, the spin configuration remains symmetry-related rather than inverted, differing by a relative rotation angle of $\pi/3$ in the low-field regime. Our results establish chiral antiferromagnets as hosts of intrinsic magnetic nonreciprocity and extend nonreciprocal phenomena from transport and propagating excitations to the quasi-static collective magnetic response of ordered quantum materials.

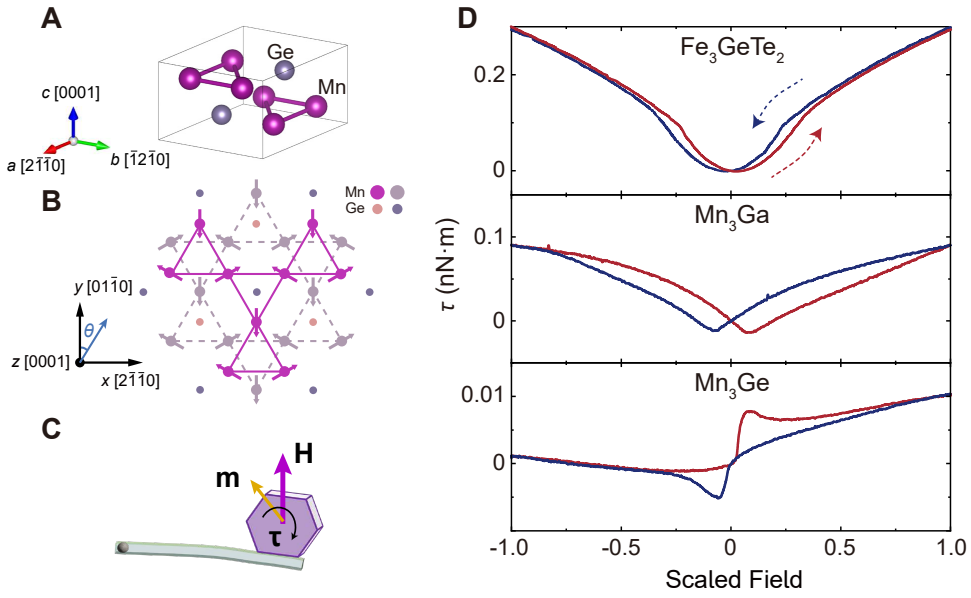


Figure 1: **Detect reciprocal and nonreciprocal magnetic response.** (**A**) Crystal structure of Mn_3Ge. The Mn Atoms form kagome lattices as shown in (**B**). The coordinate axes and corresponding crystallographic directions used in this work are defined in (**B**). (**C**) Schematic diagram of torque measurement. When rotating the sample, magnetic field is aligned within the kagome plane of Mn_3Ge. The magnetic torque vector is perpendicular to the rotation plane and therefore along c-axis of the sample. The sample is mounted by hand, which could induce a small misalignment of $<5°$. (**D**) Magnetic torque of Fe_3GeTe_2, Mn_3Ga, and Mn_3Ge measured at 10 K. **H** is along y-axis for Mn_3Ga and Mn_3Ge.

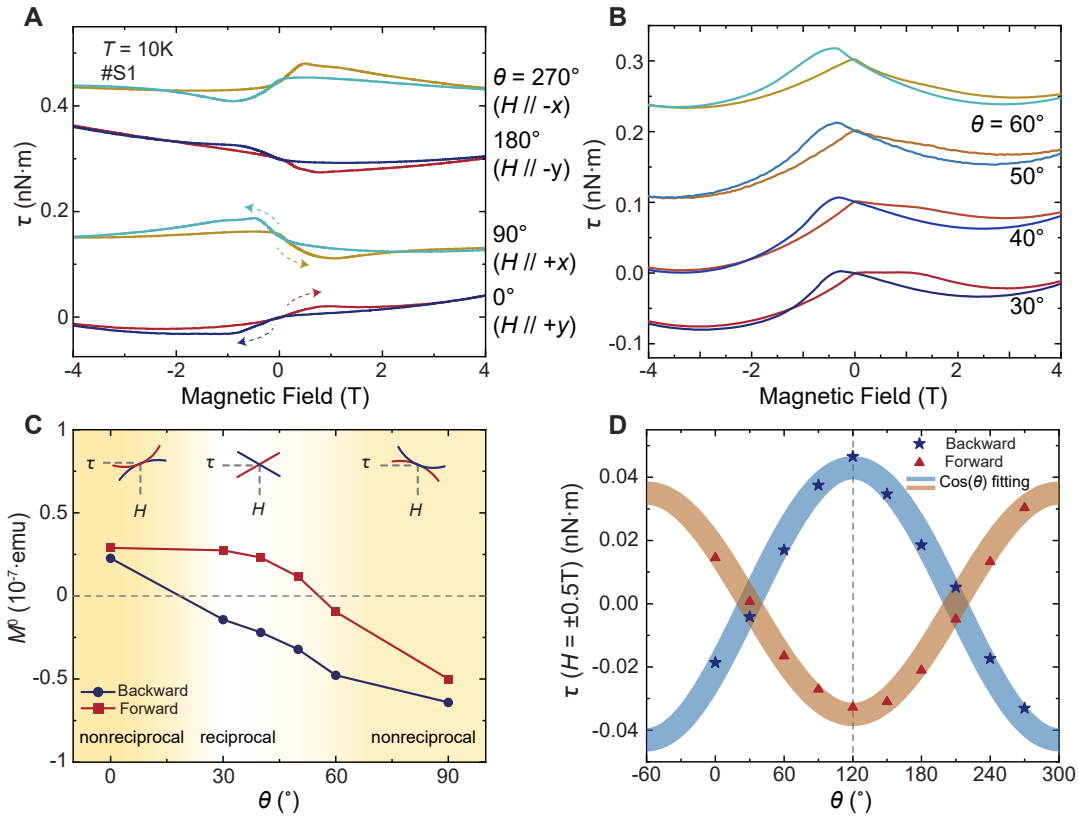


Figure 2: **Angular dependent magnetic torque measurements.** (**A**) Magnetic torque results measured at 10 K with the magnetic field orientation θ = 0°, 90°, 180°, and 270°. Each pair of curves was obtained for forward (red and yellow curves) and backward (blue and green curves) field sweeps. (**B**) Detailed angular dependent torque with θ = 30°, 40°, 50°, and 60°. Curves in (**A**) and (**B**) are offset for clarity, and $\boldsymbol{\tau}$ = 0 at zero field. (**C**) The effective spontaneous transverse moment ($M^{0,\perp}$) extracted from the low-field torque, as a function of field orientation for forward (red) and backward (blue) field sweep. The three insets demonstrate schematic diagram of torque versus magnetic field with nonreciprocal and reciprocal response. (**D**) The selected torque values at +0.5 T (for forward sweep) and −0.5 T (for backward sweep) follow a sinusoidal angular dependence expected from $\boldsymbol{\tau} \propto \mathbf{M}^0 \times \mathbf{H}$.

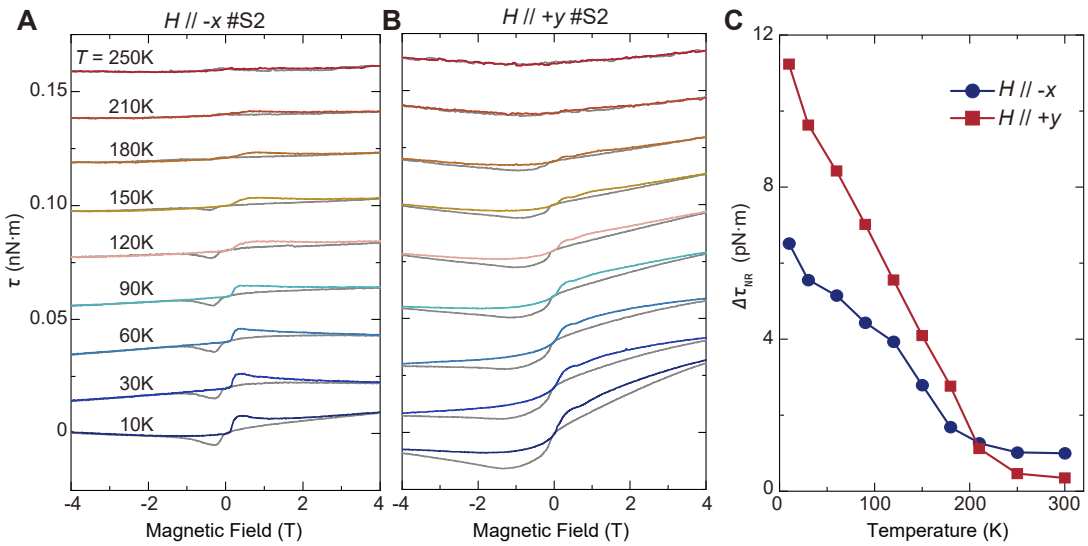


Figure 3: **Magnetic torque measurements at different temperatures.** Temperature dependent magnetic torque measurements with field along the $-x$-axis (**A**) and $+y$-axis (**B**). Both forward (colored curves) and backward (gray curves) data is presented. Above ~210 K, the nonreciprocal magnetic response behavior disappears. (**C**) The temperature dependent $\Delta\tau$ for **H** parallel to $-x$ (blue) and $+y$-axis (red). $\Delta\tau$ is defined in the main text.

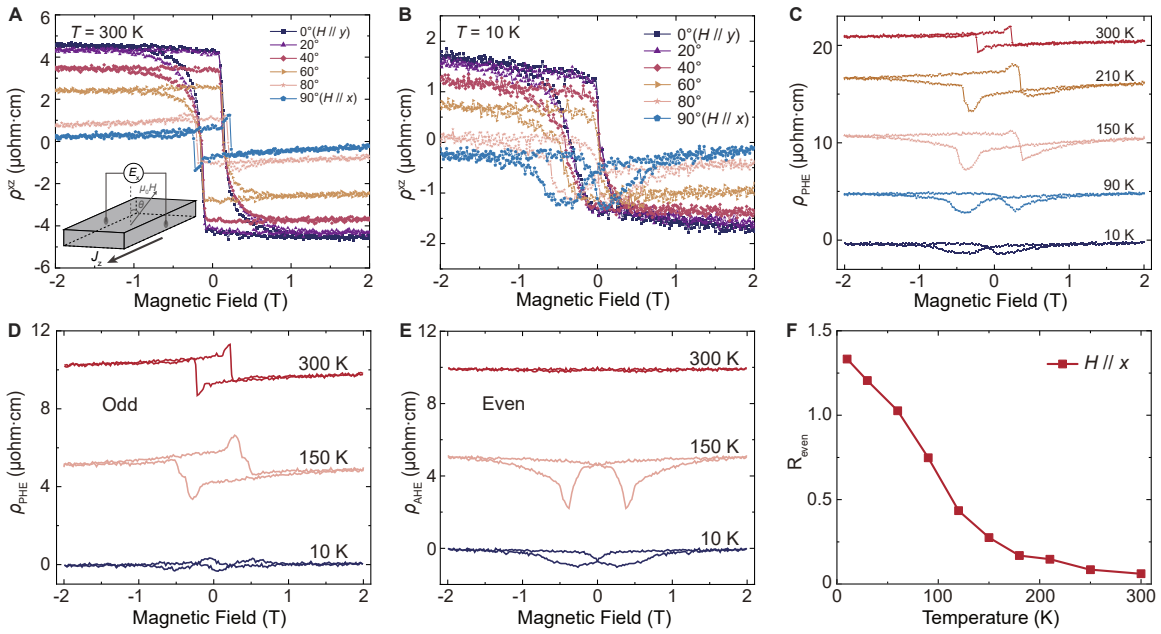


Figure 4: **Planar Hall effect and Anomalous Hall effect of Mn_3Ge.** Hall measurements of Mn_3Ge at 300 K (**A**) and 10 K (**B**) with different field orientations. The current is along z-axis and the voltage is measured along x ($[2\bar{1}\bar{1}0]$) direction. The magnetic field was rotated from $\theta = 0°$ (**H** $\parallel$ y) to 90° (**H** $\parallel$ x). For normal Hall measurement configuration (**H** $\parallel$ y), pronounced AHE is visible at both 300 K and 10 K, while for the case of planar Hall configuration (**H** $\parallel$ x), PHE is visible only at 10 K. (**C**), Raw planar Hall measurement (ρ_{PHE}) at different temperatures for **H** $\parallel$ x. The derived asymmetric and symmetric components of ρ_{PHE} versus temperature are plotted in (**D**) and (**E**), respectively. (**F**) The temperature dependent even-to-odd ratio R_{even} of Mn_3Ge.

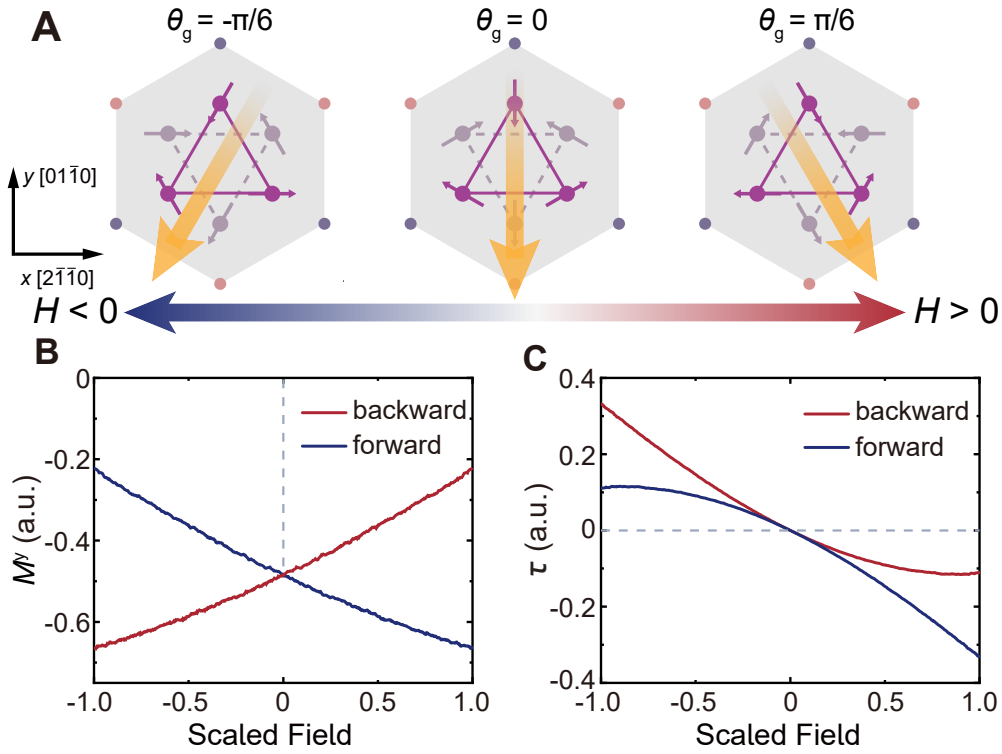


Figure 5: Theoretical model of field-induced spin reorientation and nonreciprocal response. (**A**), Evolution of the magnetic global rotating angle (θ_g) and spin configuration in Mn_3Ge as the magnetic field reverses from negative (left, $\theta_g = -\pi/6$) to positive (right, $\theta_g = \pi/6$). The orange arrows indicate the twofold rotation axis that determines the orientation of the spontaneous magnetization. (**B**), Calculated magnetization M^y versus scaled magnetic field in the low-field regime, showing an even-in-field response (symmetric hysteresis loop) for forward (blue) and backward (red) field sweeps. (**C**), Corresponding calculated torque τ showing an odd-in-field, nonreciprocal response (antisymmetric hysteresis). All data are calculated for the low-field range (corresponding to **H** < 0.5 T experimentally).

References and Notes

1. Y. Tokura, N. Nagaosa, Nonreciprocal responses from non-centrosymmetric quantum materials. *Nat. Commun.* **9** (1), 3740 (2018).

2. M. Nadeem, M. S. Fuhrer, X. Wang, The superconducting diode effect. *Nat. Rev. Phys.* **5** (10), 558–577 (2023).

3. N. Nagaosa, Y. Yanase, Nonreciprocal transport and optical phenomena in quantum materials. *Annu. Rev. Condens. Matter Phys.* **15** (1), 63–83 (2024).

4. Y. Pan, *et al.*, Helicity dependent photocurrent in electrically gated $(Bi_{1-x}Sb_x)_2Te_3$ thin films. *Nat. Commun.* **8** (1), 1037 (2017).

5. K. Kang, T. Li, E. Sohn, J. Shan, K. F. Mak, Nonlinear anomalous Hall effect in few-layer WTe_2. *Nat. Mater.* **18** (4), 324–328 (2019).

6. R. Aoki, Y. Kousaka, Y. Togawa, Anomalous Nonreciprocal Electrical Transport on Chiral Magnetic Order. *Phys. Rev. Lett.* **122** (5), 057206 (2019).

7. J. E. Sipe, A. I. Shkrebtii, Second-order optical response in semiconductors. *Phys. Rev. B* **61** (8), 5337–5352 (2000).

8. G. L. J. A. Rikken, J. Fölling, P. Wyder, Electrical Magnetochiral Anisotropy. *Phys. Rev. Lett.* **87**, 236602 (2001).

9. K. Jiang, J. Hu, Superconducting diode effects. *Nat. Phys.* **18** (10), 1145–1146 (2022).

10. C. Wu, K. Sun, E. Fradkin, S.-C. Zhang, Fermi liquid instabilities in the spin channel. *Phys. Rev. B* **75**, 115103 (2007).

11. H. Ikeda, Y. Ohashi, Theory of Unconventional Spin Density Wave: A Possible Mechanism of the Micromagnetism in U-based Heavy Fermion Compounds. *Phys. Rev. Lett.* **81**, 3723–3726 (1998).

12. L. Šmejkal, J. Sinova, T. Jungwirth, Emerging Research Landscape of Altermagnetism. *Phys. Rev. X* **12**, 040501 (2022).

13. Q. Liu, X. Dai, S. Blügel, Different facets of unconventional magnetism. *nature physics* **21** (3), 329–331 (2025).

14. H. Chen, Q. Niu, A. H. MacDonald, Anomalous Hall Effect Arising from Noncollinear Antiferromagnetism. *Phys. Rev. Lett.* **112**, 017205 (2014).

15. J. Kübler, C. Felser, Non-collinear antiferromagnets and the anomalous Hall effect. *Europhys. Lett.* **108** (6), 67001 (2014).

16. S. Nakatsuji, R. Arita, Topological Magnets: Functions Based on Berry Phase and Multipoles. *Annu. Rev. Condens. Matter Phys.* **13**, 119–142 (2022).

17. L. Šmejkal, A. H. MacDonald, J. Sinova, S. Nakatsuji, T. Jungwirth, Anomalous Hall antiferromagnets. *Nat. Rev. Mater.* **7** (6), 482–496 (2022).

18. B. H. Rimmler, B. Pal, S. S. P. Parkin, Non-collinear antiferromagnetic spintronics. *Nat. Rev. Mater.* **10** (2), 109–127 (2024).

19. H. Chen, *et al.*, Manipulating anomalous Hall antiferromagnets with magnetic fields. *Phys. Rev. B* **101**, 104418 (2020).

20. P. Liu, J. Li, J. Han, X. Wan, Q. Liu, Spin-Group Symmetry in Magnetic Materials with Negligible Spin-Orbit Coupling. *Phys. Rev. X* **12**, 021016 (2022).

21. S.-B. Zhang, L.-H. Hu, Finite-momentum mixed singlet-triplet pairing in chiral antiferromagnets induced by even-parity spin texture. *Phys. Rev. B* **112**, L100501 (2025).

22. Z. Liu, Y. Gao, Q. Niu, Rigid-Body Anisotropy in Noncollinear Antiferromagnets. *Phys. Rev. Lett.* **136**, 026703 (2026).

23. Y. Liu, *et al.*, Symmetry classification of magnetic orders using oriented spin space groups. *Nature* **652** (8111), 869–873 (2026).

24. N. L. Nair, *et al.*, Electrical switching in a magnetically intercalated transition metal dichalcogenide. *Nat. Mater.* **19** (2), 153–157 (2020).

25. E. Krén, G. Kádár, Neutron diffraction study of Mn_3Ga. *Solid State Commun.* **8** (20), 1653–1655 (1970).

26. N. Yamada, H. Sakai, H. Mori, T. Ohoyama, Magnetic properties of ϵ-Mn_3Ge. *Physica B+C* **149** (1), 311–315 (1988).

27. J. Sticht, K.-H. Höck, J. Kübler, Non-collinear itinerant magnetism: the case of Mn_3Sn. *J. Phys.: Condens. Matter* **1** (43), 8155 (1989).

28. Y. Zhang, *et al.*, Strong anisotropic anomalous Hall effect and spin Hall effect in the chiral antiferromagnetic compounds Mn_3X (X = Ge, Sn, Ga, Ir, Rh, and Pt). *Phys. Rev. B* **95**, 075128 (2017).

29. T. Chen, *et al.*, Anomalous transport due to Weyl fermions in the chiral antiferromagnets Mn_3X, X = Sn, Ge. *Nat. Commun.* **12** (1), 572 (2021).

30. S. Nakatsuji, N. Kiyohara, T. Higo, Large anomalous Hall effect in a non-collinear antiferromagnet at room temperature. *Nature* **527** (7577), 212–215 (2015).

31. K. Kuroda, *et al.*, Evidence for magnetic Weyl fermions in a correlated metal. *Nat. Mater.* **16** (11), 1090–1095 (2017).

32. M.-T. Suzuki, T. Koretsune, M. Ochi, R. Arita, Cluster multipole theory for anomalous Hall effect in antiferromagnets. *Phys. Rev. B* **95** (9), 094406 (2017).

33. M. Kimata, *et al.*, Magnetic and magnetic inverse spin Hall effects in a non-collinear antiferromagnet. *Nature* **565** (7741), 627–630 (2019).

34. H. Tsai, *et al.*, Electrical manipulation of a topological antiferromagnetic state. *Nature* **580** (7805), 608–613 (2020).

35. T. Higo, *et al.*, Perpendicular Full Switching of Chiral Antiferromagnetic Order by Current. *Nature* **607** (7919), 474–479 (2022).

36. B. Pal, *et al.*, Setting of the magnetic structure of chiral kagome antiferromagnets by a seeded spin-orbit torque. *Sci. Adv.* **8** (24), eabo5930 (2022).

37. X. Chen, *et al.*, Octupole-driven magnetoresistance in an antiferromagnetic tunnel junction. *Nature* **613** (7944), 490–495 (2023).

38. Z. Zheng, *et al.*, All-electrical perpendicular switching of chiral antiferromagnetic order. *Nat. Mater.* **24** (9), 1407–1413 (2025).

39. Y. Takeuchi, *et al.*, Electrical coherent driving of chiral antiferromagnet. *Science* **389** (6762), 830–834 (2025).

40. Z. Zhou, *et al.*, Field-free full switching of chiral antiferromagnetic order. *Nature* **651** (8105), 341–347 (2026).

41. H. Tsai, *et al.*, Picosecond ultralow-power switching device based on an antiferromagnet. *Science* **392** (6799), 761–765 (2026), doi:10.1126/science.adt3136, `https://www.science.org/doi/10.1126/science.adt3136`.

42. N. Kiyohara, T. Tomita, S. Nakatsuji, Giant Anomalous Hall Effect in the Chiral Antiferromagnet Mn_3Ge. *Phys. Rev. Appl.* **5** (6), 064009 (2016).

43. A. K. Nayak, *et al.*, Large anomalous Hall effect driven by a nonvanishing Berry curvature in the noncolinear antiferromagnet Mn_3Ge. *Sci. Adv.* **2** (4), e1501870 (2016).

44. L. Song, *et al.*, Large Anomalous Hall Effect at Room Temperature in a Fermi-Level-Tuned Kagome Antiferromagnet. *Adv. Funct. Mater.* **34**, 2316588 (2024).

45. R. Okazaki, *et al.*, Rotational Symmetry Breaking in the Hidden-Order Phase of URu_2Si_2. *Science* **331** (6016), 439–442 (2011).

46. T. Asaba, *et al.*, Evidence for an odd-parity nematic phase above the charge-density-wave transition in a kagome metal. *Nat. Phys.* **20** (1), 40–46 (2024).

47. T. F. Duan, *et al.*, Magnetic anisotropy of single-crystalline Mn_3Sn in triangular and helix-phase states. *Appl. Phys. Lett.* **107** (8), 082403 (2015).

48. P. J. W. Moll, *et al.*, Magnetic torque anomaly in the quantum limit of Weyl semimetals. *Nat Commun* **7** (1), 12492 (2016).

49. Y. Liu, *et al.*, Probing magnetic anisotropy in Kagome antiferromagnetic Mn_3Ge with torque magnetometry. *J. Magn. Magn. Mater.* **563**, 170018 (2022).

50. J. M. Coey, *Magnetism and magnetic materials* (Cambridge University Press) (2010).

51. E. Krén, G. Kádár, Neutron diffraction study of Mn_3Ga. *Solid State Commun.* **8** (20), 1653–1655 (1970).

52. Y. Deng, *et al.*, Gate-tunable room-temperature ferromagnetism in two-dimensional Fe_3GeTe_2. *Nature* **563** (7729), 94–99 (2018).

53. L. Xu, *et al.*, Finite-temperature violation of the anomalous transverse Wiedemann-Franz law. *Sci. Adv.* **6** (17), eaaz3522 (2020).

54. X. Li, *et al.*, Chiral domain walls of Mn_3Sn and their memory. *Nat. Commun.* **10** (1), 3021 (2019).

55. L. Xu, X. Li, L. Ding, K. Behnia, Z. Zhu, Planar Hall effect caused by the memory of antiferromagnetic domain walls in Mn_3Ge. *Appl. Phys. Lett.* **117** (22), 222403 (2020).

56. Materials and methods are available as supplementary materials.

57. L.-H. Hu, S.-B. Zhang, Spin magnetization in unconventional antiferromagnets with collinear and non-collinear spins. *Sci. China-Phys. Mech. Astron.* **68** (4), 247211 (2025).

58. M. Wu, *et al.*, Current-driven fast magnetic octupole domain-wall motion in noncollinear antiferromagnets. *Nat. Commun.* **15** (1), 4305 (2024).

59. J. C. Slater, G. F. Koster, Simplified LCAO Method for the Periodic Potential Problem. *Phys. Rev.* **94**, 1498–1524 (1954).

60. S. Konschuh, M. Gmitra, J. Fabian, Tight-binding theory of the spin-orbit coupling in graphene. *Phys. Rev. B* **82**, 245412 (2010).

61. Z. Liu, *et al.*, Multipolar Anisotropy in Anomalous Hall Effect from Spin-Group Symmetry Breaking. *Phys. Rev. X* **15**, 031006 (2025).

Acknowledgments

We sincerely thank Song Bao, Zihang Song and Jinsheng Wen at Nanjing University for supporting the Laue diffraction measurements. We acknowledge fruitful discussions with Qian Niu and Yang Gao.

Funding: This work was supported by the National Key R&D Program of China (Grant Nos. 2022YFA1402200, 2023YFA1406100, and 2023YFA1406600), the Zhejiang Provincial Natural Science Foundation of China (Grant No. LR25A040003), and the National Natural Science Foundation of China (Grants Nos. 12374151, 12034017, 12274068, and 12350710785).

Author contributions: L.J, L.H., and H.Y conceived the project. H.G., Z.S., J.L.Z, and Y.J.L. performed experimental measurements. T.C. L.Y., and J.W.Z. provided samples. Z.W., K.X., and L.H. performed theoretical analysis. H.G., L.J., and L.H. wrote the manuscript with the input of all authors.

Competing interests: The authors declare no competing interests.

Data and materials availability: The experimental data and theory code of this study will be available on public repository.

Supplementary Files

This is a list of supplementary files associated with this preprint. Click to download.

- Mn3GeSM.pdf